

# Collective Ratchet Effects and Reversals for Active Matter Particles on Quasi-One-Dimensional Asymmetric Substrates

Danielle McDermott,<sup>1,2</sup> Cynthia J. Olson Reichhardt,<sup>\*1</sup> and Charles Reichhardt<sup>1</sup>

Received Xth XXXXXXXXXX 20XX, Accepted Xth XXXXXXXXXX 20XX

First published on the web Xth XXXXXXXXXX 200X

DOI: 10.1039/b000000x

Using computer simulations, we study a two-dimensional system of sterically interacting self-mobile run-and-tumble disk-shaped particles with an underlying periodic quasi-one-dimensional asymmetric substrate, and show that a rich variety of collective active ratchet behaviors arise as a function of particle density, activity, substrate strength, and substrate period. The ratchet efficiency is nonmonotonic since the ratcheting is enhanced by increased activity but diminished by the onset of self-clustering of the active particles. Increasing the particle density decreases the ratchet efficiency for weak substrates but increases the ratchet efficiency for strong substrates due to collective hopping events. At the highest particle densities, the ratchet motion is destroyed by a self-jamming effect. We show that it is possible to realize reversals of the ratchet effect, where the net flux of particles is along the hard rather than the easy direction of the substrate asymmetry. The reversals occur in the strong substrate limit when multiple rows of active particles can be confined in each substrate minimum, permitting emergent particle-like excitations to appear that experience an inverted effective substrate potential. We map out a phase diagram of the forward and reverse ratchet effects as a function of the particle density, activity, and substrate properties.

## 1 Introduction

A nonequilibrium assembly of particles subjected to a driving force that, by itself, produces no net motion can exhibit a net dc drift called a ratchet effect when enough symmetries are broken, such as by the introduction of an asymmetric substrate. A wide variety of ratchet effects are possible, including a rocking ratchet for particles driven over an asymmetric substrate by an ac force, or a flashing ratchet for thermally fluctuating particles interacting with a substrate that is switched on and off periodically<sup>1–3</sup>. Ratchet effects produced using asymmetric substrates have been studied in a wide range of systems including colloidal particles<sup>4</sup>, vortices in type-II superconductors<sup>5,6</sup>, magnetic domain walls<sup>7,8</sup>, polymers<sup>9,10</sup>, granular matter<sup>11,12</sup>, and cold atoms<sup>13</sup>. Systems with symmetric substrates can also exhibit ratchet effects if additional asymmetry is introduced, such as from an asymmetric external driving force<sup>14–16</sup>. For overdamped non-interacting particles on an asymmetric substrate, the normal ratchet effect creates a particle drift in the easy flow direction of the substrate asymmetry. Interacting particle systems can exhibit a reversal, or even multiple reversals, of the ratchet effect in which the net drift is in the hard direction of the substrate asymmetry<sup>17</sup>. Ratchet

reversals have been observed in rocking ratchets for interacting superconducting vortices in asymmetric pinning arrays as a function of vortex density or ac drive amplitude<sup>18–22</sup>. While in these systems some form of external driving must be applied to produce the ratchet effect, for self-propelled particles, known as active matter<sup>23–25</sup>, ratchet effects can appear in the absence of external driving<sup>26–30</sup>.

Rectification effects in active matter systems were first observed for run-and-tumble swimming bacteria moving through an array of funnel-shaped barriers<sup>26</sup>. The initially uniformly distributed bacteria become concentrated on the easy flow side of the funnels over time, while non-swimming bacteria undergo no rectification<sup>26</sup>. Subsequent simulations of run-and-tumble particles in similar funnel geometries produced a similar ratchet effect caused by the interaction of the running particles with the asymmetric funnel walls, while the ratchet effect disappeared in the Brownian limit of very short running times<sup>27</sup>. Further studies showed that this rectification effect depends on the nature of the particle interactions with the barriers; a ratchet effect can occur when detailed balance is broken, but is absent when the particles scatter elastically from the barriers<sup>28</sup>. Active ratchets have been studied for a variety of self-driven systems in the presence of asymmetric substrates<sup>31–34</sup> or asymmetric obstacles<sup>35–37</sup>, as well as for more complicated self-driven systems such as active ellipsoids<sup>38</sup>, active polymers<sup>39</sup>, and self-driven Janus particles<sup>40</sup> on asymmetric substrates. Other studies have shown how active ratchet effects can be exploited to transport non-active

<sup>1</sup> Theoretical Division, Los Alamos National Laboratory, Los Alamos, New Mexico 87545 USA. Fax: 1 505 606 0917; Tel: 1 505 665 1134; E-mail: [cjrx@lanl.gov](mailto:cjrx@lanl.gov)

<sup>2</sup> Department of Physics, Wabash College, Crawfordsville, Indiana 47933 USA.

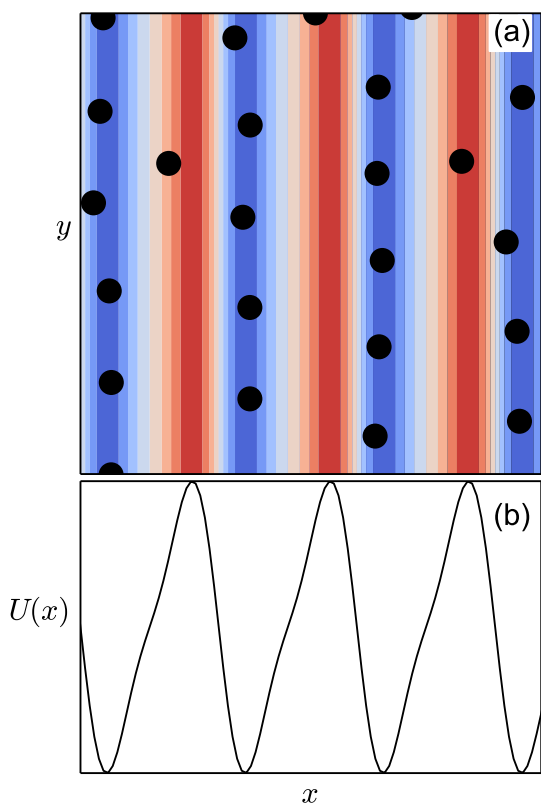


**Fig. 1** (a) Top view of a portion of the asymmetric potential  $U(x)$ , where red (blue) shading indicates high (low) potential energy. The black circles schematically show the locations of the self-propelled particles. (b) The corresponding shape of the potential  $U(x)$  vs  $x$ .

colloidal cargo<sup>41</sup>, rotate asymmetric gears immersed in active matter<sup>42,43</sup>, capture active particles with asymmetric traps<sup>44</sup>, and direct the motion of asymmetric obstacles in active matter baths<sup>45,46</sup>.

When interactions between active matter particles are included, dynamical effects such as self-trapping<sup>47</sup> and clustering effects<sup>48–51</sup> arise even in the absence of a substrate. Recent simulations of disk-shaped active particles driven through an array of obstacles show that the drift velocity of the particles initially increases with increasing activity, but decreases with increasing activity once self-clustering or self-jamming begins to occur<sup>52</sup>. It might be expected that active matter ratchet effects would generally diminish when particle-particle interactions are introduced, as observed by Wan *et al.* for run-and-tumble particles moving through a funnel array, where the ratchet effect decreased with increasing particle density<sup>27</sup>. This is, however, not always the case. For active matter particles on asymmetric substrates, reversals in the ratchet effect have been observed for interacting particles obeying a flocking or Vicsek model<sup>53</sup> that move through an array of funnel bar-

riers<sup>54</sup> as well as in experiments on eukaryotic cells crawling through asymmetric channels<sup>55</sup>. For simpler systems such as self-propelled disks or rods on asymmetric substrates, ratchet reversals have not yet been observed.

In this work we examine a two-dimensional (2D) system of sterically interacting run-and-tumble disk-shaped particles moving over an asymmetric quasi-one-dimensional periodic substrate. At low particle densities, a ratchet effect occurs in the easy flow direction of the substrate asymmetry. For weak substrates, the ratchet efficiency increases with increasing run time, and it decreases with increasing particle density when self-clustering occurs. For stronger substrates, the ratchet efficiency is a nonmonotonic function of particle density and run time. When the substrate is strong enough to confine multiple rows of particles in each potential minimum, multi-body collisions can occur that push particles over the substrate barriers, generating a reversed ratchet effect with motion in the hard direction of the substrate asymmetry. This reversed ratchet effect is suppressed at high particle densities when self-clustering occurs, and it also disappears for very strong substrates when the particles form one-dimensional rows in which multi-body collisions do not occur. A transition from a reverse to a normal ratchet effect can occur when the run time is increased. We describe the direction and efficiency of the ratchet effect in a series of phase diagrams as functions of the particle density, run time, substrate strength, and substrate periodicity.

## 2 Simulation and System

We consider a 2D system of size  $L \times L$  with periodic boundary conditions in the  $x$ - and  $y$ -directions containing  $N$  self-propelled disk-shaped particles. The steric particle-particle interactions are modeled as a harmonic repulsive potential which drops to zero beyond the particle radius  $r_d$ . We take  $r_d = 0.5$  and  $L = 36$  in dimensionless simulation length units. The particle density  $\phi$  is given by the total fraction of the sample area covered by the particles,  $\phi = N\pi r_d^2/L^2$ . The highest possible particle density in 2D is a triangular solid with  $\phi = 0.9$ . The dynamics of a particle  $i$  is governed by the following overdamped equation of motion:

$$\eta \frac{d\mathbf{r}_i}{dt} = \mathbf{F}_i^m + \mathbf{F}_i^{in} + \mathbf{F}_i^{sub}. \quad (1)$$

Here  $\eta$  is the damping constant, which is set equal to unity. The self-propulsion is modeled using run-and-tumble dynamics in which the motor force  $\mathbf{F}_i^m$  is fixed to a randomly chosen direction during a running time  $\tau$ , after which a new randomly chosen direction is selected for the next running time  $\tau$ . We take the magnitude of the motor force to be  $F_m = 1.0$ . In the absence of any other interactions, during a single run interval a particle travels a distance  $R_l = F_m \tau \Delta t$ , where  $\Delta t = 0.002$  is the size of the simulation time step. The steric particle-particle

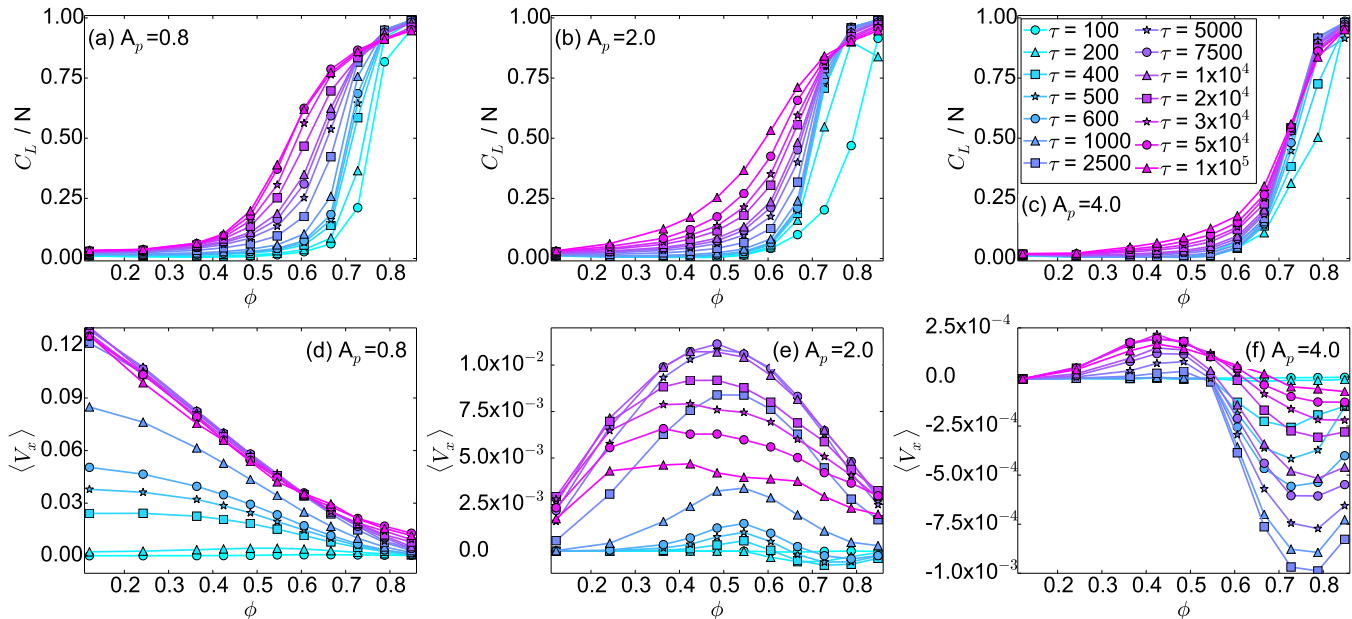


**Fig. 2** (a,b,c) The average cluster size  $C_L/N$  vs particle density  $\phi$ . (d,e,f) The average particle velocity  $\langle V_x \rangle$  vs  $\phi$ . The color code, shown in panel (f), indicates different run times  $\tau = 100, 200, 400, 500, 600, 1000, 2500, 5000, 7500, 1 \times 10^4, 2 \times 10^4, 3 \times 10^4, 5 \times 10^4$ , and  $1 \times 10^5$ . (a,d) At  $A_p = 0.8$ , there is a normal ratchet effect with an efficiency that decreases with increasing  $\phi$ . (b,e) At  $A_p = 2.0$ , the efficiency of the normal ratchet effect is nonmonotonic, so that the ratcheting is optimized for a midrange value of  $\phi$ . (c,f) At  $A_p = 4.0$ , there is a crossover from a normal to a reverse ratchet effect with increasing  $\phi$ .

interaction force is  $F_{ij}^{in} = \sum_{i \neq j}^N k(2r_d - |\mathbf{r}_{ij}|)\Theta(2r_d - |\mathbf{r}_{ij}|)\hat{\mathbf{r}}_{ij}$  where  $\mathbf{r}_{ij} = \mathbf{r}_i - \mathbf{r}_j$ ,  $\hat{\mathbf{r}}_{ij} = \mathbf{r}_{ij}/|\mathbf{r}_{ij}|$ ,  $\Theta$  is the Heaviside step function, and the spring constant  $k = 30$ . The substrate force  $\mathbf{F}_i^{sub} = -\nabla U(x_i)\hat{\mathbf{x}}$  arises from an asymmetric potential of the form

$$U(x) = U_0[\sin(2\pi x/a) + 0.25\sin(4\pi x/a)] \quad (2)$$

where  $a$  is the substrate period and the substrate strength is defined to be  $A_p = 2\pi U_0/a$ . Unless otherwise noted, we take  $a = 1.0$ . A small section of  $U(x)$  is illustrated in Fig. 1. To quantify the ratchet effect, we measure the net velocity per particle in the  $x$  direction,  $\langle V_x \rangle = N^{-1} \sum_{i=1}^N \mathbf{v}_i \cdot \hat{\mathbf{x}}$ , where  $\mathbf{v}_i$  is the velocity of particle  $i$ . We average  $\langle V_x \rangle$  over at least  $10^7$  simulation time steps to ensure that we are obtaining a steady state measurement. We vary  $\phi$ ,  $A_p$ ,  $a$ , and  $\tau$  and measure the resulting direction and efficiency of the ratcheting behavior.

### 3 Results

In Fig. 2(a) we plot the normalized size of the largest particle cluster  $C_L/N$  versus  $\phi$  for varied run times  $\tau$  at a fixed substrate strength of  $A_p = 0.8$ . A group of  $n$  particles that are all in physical contact with each other is defined to be a cluster of size  $C_L = n$ . We measure  $C_L$  using the algorithm described

in<sup>56</sup>, and define the system to be in a self-clustering state when  $C_L/N > 0.5$ . As  $\tau$  increases, the onset of self-clustering shifts to lower values of  $\phi$ , in agreement with earlier studies showing that clustering occurs at lower densities when the run time<sup>52</sup> or the persistence length<sup>48,49</sup> of the motor force is increased. Figure 2(d) shows the corresponding values of  $\langle V_x \rangle$  versus  $\phi$ . For the lowest value of  $\tau = 100$ , the system is in the Brownian limit and  $\langle V_x \rangle = 0$  for all values of  $\phi$ , while at higher run times, the system exhibits a normal ratchet effect. In this weak substrate regime, we find that  $\langle V_x \rangle$  decreases with increasing  $\phi$  and increases with increasing  $\tau$ , with a saturation for  $\tau > 5000$  as shown in Fig. 2(d). This result is in agreement with the studies of Wan *et al.* on interacting active particles in funnel arrays, where the magnitude of the ratchet effect increases with increasing  $\tau$  before reaching a plateau at large  $\tau$ , and decreases with increasing particle density<sup>27</sup>. For the system in Fig. 2(a,d), at low  $\phi$  very few particle-particle collisions occur, making the behavior similar to that of a single particle, which moves further along the easy direction of the substrate asymmetry than along the hard direction since  $F^m > A_p$ . As  $\phi$  increases, two effects combine to reduce the magnitude of the forward ratchet effect. The particles collide more often, producing a more thermal distribution of particle motion, while individual particles are more likely to become trapped inside a cluster, therefore becoming unavailable for hopping over the

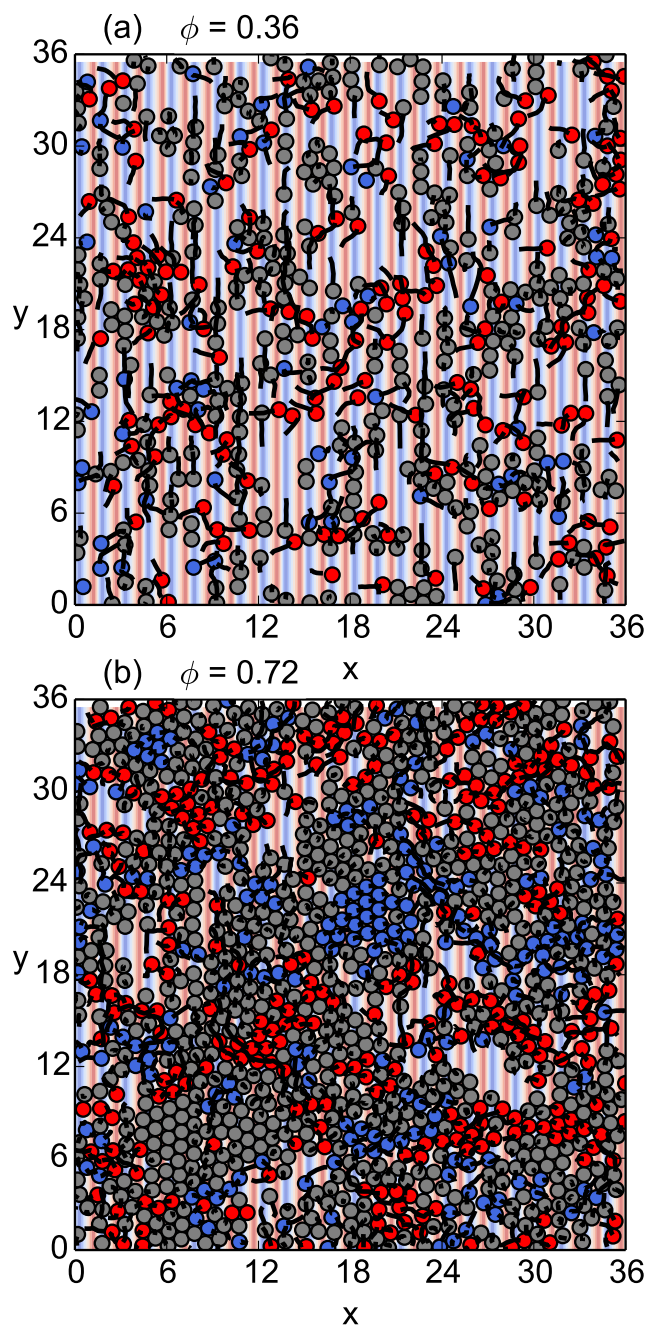


**Fig. 3** Active particle positions (circles) and trajectories (black lines), along with the underlying substrate potential (red and blue lines), at  $A_p = 0.8$  and  $\tau = 10^5$  for the system in Fig. 2(a,d). Red particles have moved a distance  $\Delta x \geq a/4$  in the forward (positive  $x$ ) direction during the illustrated time interval, while blue particles have moved a distance  $\Delta x \geq a/4$  in the reverse (negative  $x$ ) direction; gray particles have moved a distance  $\Delta x < a/4$ . (a) At  $\phi = 0.36$ , there is a large normal ratchet effect and few clusters are present. (b) At  $\phi = 0.72$ , self-cluster formation suppresses the ratchet effect.

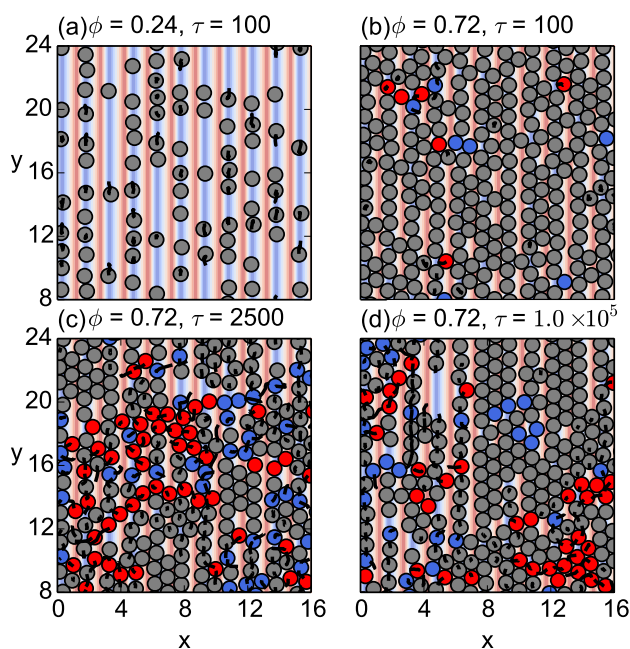


**Fig. 4** Active particle positions (circles) and trajectories (black lines), along with the underlying substrate potential (red and blue lines), in a portion of the sample for the system in Fig. 2(b,e) with  $A_p = 2.0$ . Particles are colored as in Fig. 3. (a) At  $\phi = 0.24$  and  $\tau = 100$ ,  $\langle V_x \rangle = 0$  and the particles are trapped in the substrate minima. (b) At  $\phi = 0.72$  and  $\tau = 100$ , a uniform pinned state forms with  $\langle V_x \rangle = 0$ . (c) At  $\phi = 0.72$  and  $\tau = 2500$ , a normal ratchet effect occurs. (d) At  $\phi = 0.72$  and  $\tau = 1.0 \times 10^5$ , the occurrence of clustering reduces the magnitude of the normal ratchet effect.

substrate barrier.

In Fig. 3 we show the particle positions and trajectories for the weak substrate system from Fig. 2(a,d) with  $A_p = 0.8$  at  $\tau = 10^5$ . At  $\phi = 0.36$ , there is a large normal ratchet effect and Fig. 3(a) shows that few clusters are present. Particles that have moved a distance  $\Delta x \geq a/4$  in the easy (positive  $x$ ) direction are colored red, while those that have moved a distance  $\Delta x \geq a/4$  in the hard (negative  $x$ ) direction are colored blue. As indicated in Fig. 3(a), particles are frequently able to hop over the substrate barriers, and due to the substrate asymmetry, hops in the easy direction occur more often than hops in the hard direction, leading to a net normal ratchet effect. At  $\phi = 0.72$ , shown in Fig. 3(b), strong self-clustering is present and the normal ratchet effect is much weaker. Due to the clustering, the particles tend to move collectively at this density, and large regions of the system become jammed, with particles unable to hop over substrate barriers in either direction. The high particle density also tends to nullify the effectiveness of the substrate asymmetry, so that the few particles that are still able to hop over barriers have a nearly equal proba-



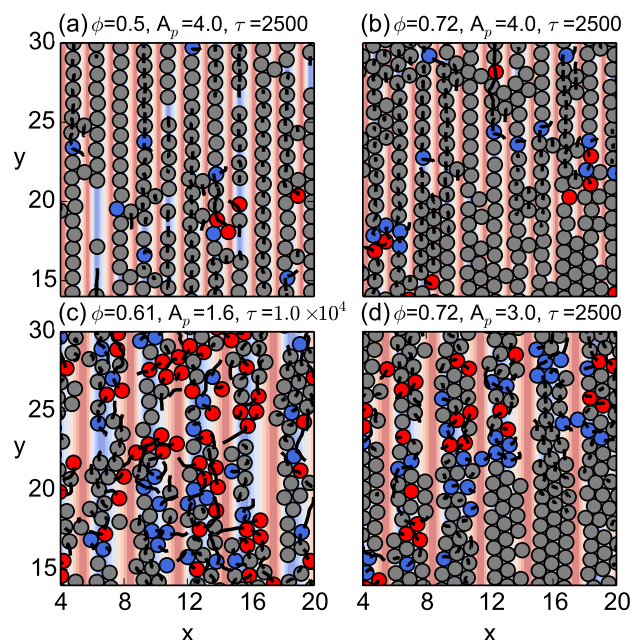


**Fig. 5** Active particle positions (circles) and trajectories (black lines), along with the underlying substrate potential (red and blue lines), in a portion of the sample. Particles are colored as in Fig. 3. (a) For  $A_p = 4.0$ ,  $\phi = 0.5$ ,  $a = 1.0$ , and  $\tau = 2500$ , the particles form 1D chains in each substrate minimum and there is a weak normal ratchet effect. (b) At  $A_p = 4.0$ ,  $\phi = 0.72$ ,  $a = 1.0$ , and  $\tau = 2500$ , each substrate minimum contains one full row of particles along with a partial second row, and a reverse ratchet effect occurs. (c) Normal ratcheting motion for  $A_p = 1.6$ ,  $\phi = 0.61$ ,  $a = 2.0$ , and  $\tau = 1 \times 10^4$ . (d) Reverse ratcheting motion for  $A_p = 3.0$ ,  $\phi = 0.72$ ,  $a = 2.0$ , and  $\tau = 2500$ .

bility of hopping in the easy direction as in the hard direction, destroying the ratchet effect.

In Fig. 2(b,e) we plot  $C_L/N$  and  $\langle V_x \rangle$  versus  $\phi$  at a higher substrate strength of  $A_p = 2.0$  for varied  $\tau$ . We again find that  $C_L/N$  increases with increasing  $\phi$  and that the onset of clustering drops to lower values of  $\phi$  as  $\tau$  increases. For the lowest value of  $\tau$ ,  $\langle V_x \rangle = 0$ , and the maximum value of  $\langle V_x \rangle$  increases with increasing  $\tau$  up to a saturation value of  $\tau = 7500$ , above which it decreases with increasing  $\tau$ , indicating that there is a run time that optimizes the ratchet efficiency. As a function of  $\phi$ ,  $\langle V_x \rangle$  is nonmonotonic, starting from a low value in the single particle limit at low  $\phi$ , and then increasing to a maximum value at the optimum density of  $\phi^* = 0.55$  before decreasing again. The value of  $\phi^*$  shifts to slightly lower densities as  $\tau$  increases. The nonmonotonic behavior of  $\langle V_x \rangle$  arises due to a competition between different collective effects. Since  $A_p > F^m$ , isolated particles cannot hop over the substrate barriers in either direction, so that  $\langle V_x \rangle = 0$  at low  $\phi$  in the single

particle limit. As  $\phi$  increases, the increased chance for collisions permits a collective barrier hopping process to occur in which interactions between multiple particles permit at least one of the particles to hop over a substrate barrier, preferentially in the easy direction of the substrate asymmetry. For  $A_p \leq F^m$ , interactions between pairs of particles is enough to permit motion in the easy direction to occur, but for  $A_p > F^m$ , three-body collisions are required to push at least one particle into a neighboring substrate minimum, preferentially on the easy direction side. At low density the three-body interactions cannot occur and there is no ratcheting effect, but as  $\phi$  increases the magnitude of the normal ratchet effect increases up to  $\phi \approx 0.5$ . Above this density, the particle-particle interactions overwhelm the substrate asymmetry as described above for the  $A_p = 0.8$  case, bringing the rate of forward hopping down until it equals the rate of backward hopping and the ratchet effect is lost.

In Fig. 4 we show the particles and trajectories for the system in Fig. 2(b,e) with  $A_p = 2.0$ . At  $\phi = 0.24$  and  $\tau = 100$ , shown in Fig. 4(a), the particles remain confined in the substrate potential minima and  $\langle V_x \rangle = 0$ . At  $\phi = 0.72$  and  $\tau = 100$ , shown in Fig. 4(b), we still find  $\langle V_x \rangle = 0$ , and the particles form a uniform pinned state. When clustering first begins at  $\phi = 0.72$  for  $\tau = 2500$ , there is a normal ratchet effect illustrated in Fig. 4(c), while for  $\phi = 0.72$  and a higher run time of  $\tau = 1 \times 10^5$ , Fig. 4(d) indicates that large numbers of clusters form in the system and interfere with the normal ratchet effect, reducing its magnitude.

In Fig. 2(c,f) we show  $C_L/N$  and  $\langle V_x \rangle$  versus  $\phi$  for a variety of  $\tau$  values in the strong substrate limit of  $A_p = 4.0$ . Here the  $C_L/N$  curves show little variation with  $\tau$  since the arrangement of the particles is dominated by the substrate minima. At the smallest values of  $\phi$ , the particles are strongly trapped in the substrate minima and  $\langle V_x \rangle = 0$ . For  $0.2 < \phi < 0.6$ , we observe a normal ratchet effect with a maximum efficiency near  $\phi = 0.4$ . A reverse ratchet effect appears for  $\phi \geq 0.6$  that is most pronounced for  $\tau = 2500$  and decreases in magnitude for larger  $\tau$ .

In Fig. 5(a) we show that at  $A_p = 4.0$ ,  $\phi = 0.5$ , and  $\tau = 2500$ , the particles form 1D chains in each substrate minimum and a weak normal ratchet effect occurs. At  $\phi = 0.72$  and  $\tau = 2500$ , where a reverse ratchet effect occurs, Fig. 5(b) shows that the particles have buckled out of the bottom of the substrate minima to form two partial rows of particles. The reversal of the ratchet effect as a function of  $\phi$  occurs when the buckling of the particles in the substrate potential causes particle-particle interactions instead of particle-substrate interactions to dominate the particle motion. When the substrate is strong, for low  $\phi$  each substrate minimum captures a single row of particles. Although isolated particles show no ratcheting behavior, when pairs of particles can come into contact along the  $y$  direction, one member of the pair can escape into

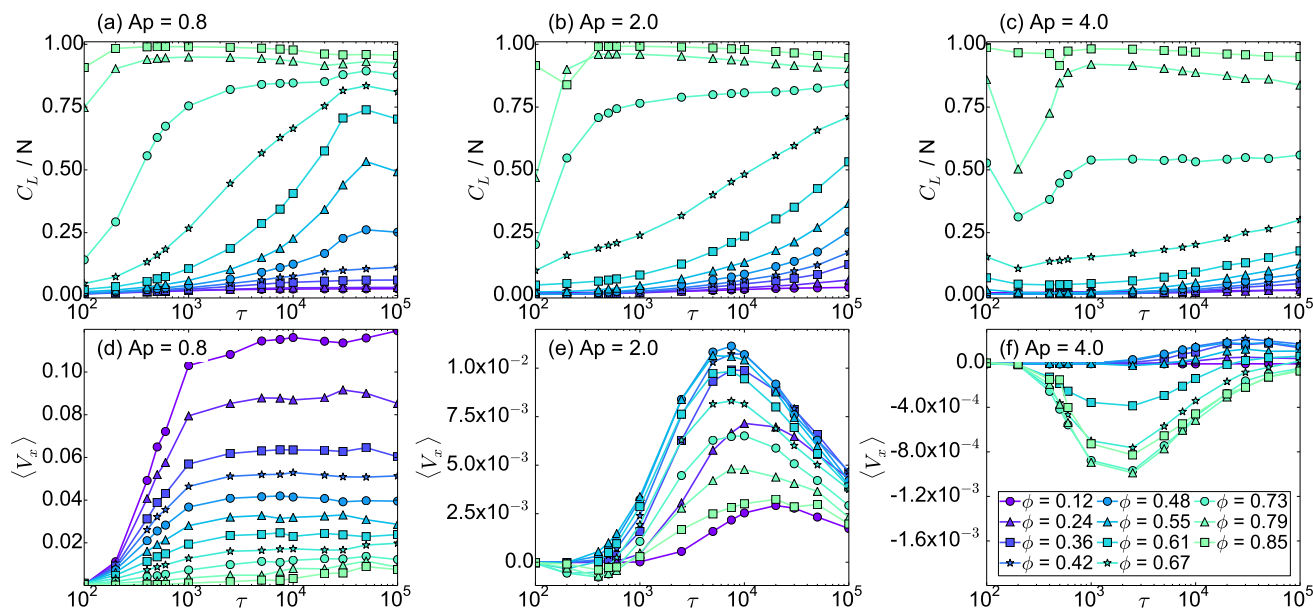


**Fig. 6** (a,b,c)  $C_L/N$  vs  $\tau$  and (d,e,f)  $\langle V_x \rangle$  vs  $\tau$  for  $\phi = 0.12, 0.24, 0.36, 0.42, 0.48, 0.55, 0.61, 0.67, 0.73, 0.79$ , and  $0.85$ . (a,d)  $A_p = 0.8$ . (b,e)  $A_p = 2.0$ . (c,f)  $A_p = 4.0$ , where a reverse ratchet effect can occur.

a neighboring substrate minimum, preferentially on the easy direction side, producing a weak normal ratchet effect. For  $\phi \geq 0.5$ , a single row of particles can no longer fit in each substrate minima, and the particles buckle to form one nearly complete row and a second partial row. The nearly complete row rests on the hard side of the substrate minimum since this provides a stronger confinement, while the partial row rests on the easy side of the substrate minimum. The effective asymmetry of the potential is reversed since the difference in slopes on the hard and easy sides of the substrate minimum becomes unimportant at these high densities, and instead, the physical distance to the substrate maximum becomes the dominant effect. The maximum is closer to the minimum in the hard direction than in the easy direction, so hopping in the hard direction is favored at large  $\phi$ , producing a reverse ratchet effect. As  $\phi$  is further increased, the substrate minimum becomes filled with particles and the asymmetry in the distance to the substrate maximum becomes less important in determining the hopping direction, causing a decrease in the efficiency of the reverse ratchet, as shown in Fig. 2(f) for  $\phi > 0.7$ . Similarly, the reverse ratchet effect becomes very weak at large values of  $\tau$  when the local asymmetry in the distance to the substrate maximum becomes unimportant.

In Fig. 6 we show  $C_L/N$  and  $\langle V_x \rangle$  as a function of  $\tau$  for varied  $\phi$  at different substrate strengths. At  $A_p = 0.8$  in Fig. 6(a),  $C_L/N$  increases with increasing  $\tau$  at low  $\phi$  but saturates to  $C_L/N \approx 1.0$  at high  $\phi$ . In Fig. 6(d), the corresponding  $\langle V_x \rangle$  curves increase with increasing  $\tau$  up to a plateau, while the

average value of  $\langle V_x \rangle$  drops as  $\phi$  increases, indicating that for weak substrates with  $0 < A_p < 1.0$ , self-clustering suppresses the normal ratchet effect by nullifying the substrate asymmetry. At  $A_p = 2.0$  in Fig. 6(e),  $\langle V_x \rangle$  is nonmonotonic, with a peak in the magnitude of the ratchet effect for  $5000 < \tau < 1 \times 10^4$ , and a decrease in  $\langle V_x \rangle$  at large values of  $\tau$  due to the occurrence of self-clustering. For high densities of  $\phi > 0.67$ , there is a window at small  $\tau$  in which a reverse ratchet effect appears caused by particles hopping over the closest maximum instead of traveling up the least steep side of the potential. Figure 6(c,f) shows  $C_L/N$  and  $\langle V_x \rangle$  versus  $\tau$  for  $A_p = 4.0$ . There is a normal ratchet effect at large  $\tau$  for  $\phi < 0.55$  and a reverse ratchet effect at intermediate  $\tau$  for  $\phi \geq 0.55$ . The efficiency of the reverse ratchet is highest at  $\tau \approx 5000$ .

For substrate strengths of  $1.6 < A_p < 4.0$ , a crossover from a reverse to a normal ratchet effect can occur as a function of  $\tau$ , as highlighted in Fig. 7(a,d), where we plot  $C_L/N$  and  $\langle V_x \rangle$  versus  $\tau$  for a sample with  $A_p = 2.5$ . There is a clear transition from a reverse ratchet to a normal ratchet effect with increasing  $\tau$ , suggesting that in a system composed of two species of particles with different  $\tau$ , it could be possible to have the two species exhibit a net drift in opposite directions.

In Fig. 7(b,e) we show  $C_L/N$  and  $\langle V_x \rangle$  versus  $A_p$  for varied  $\tau$  at  $\phi = 0.36$ , while in Fig. 7(c,f) we show the same measures at  $\phi = 0.61$ . In Fig. 7(b) at  $\phi = 0.36$ , the particle density is too low for large clusters to appear, while in Fig. 7(c) at  $\phi = 0.61$ , the clustering that occurs for low  $A_p$  is suppressed as the substrate strength is increased. At  $A_p = 0$  in Fig. 7(e,f),  $\langle V_x \rangle = 0$ ,

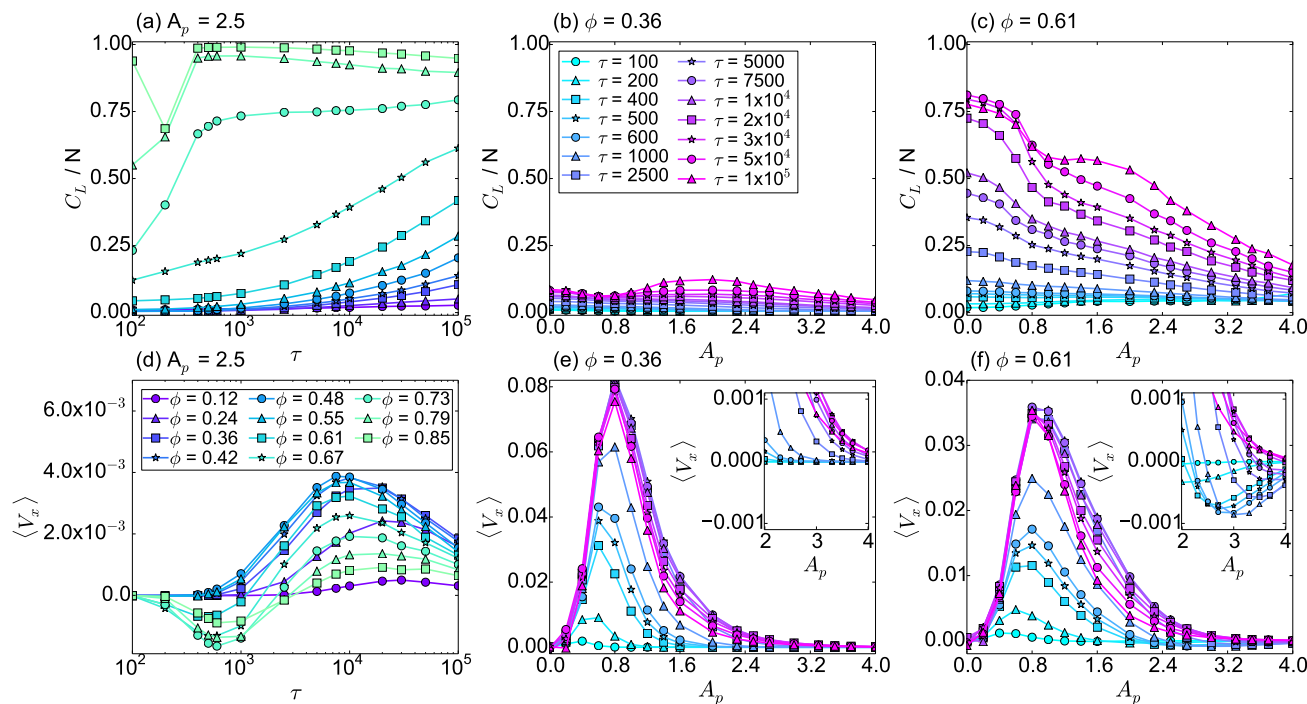


**Fig. 7** (a)  $C_L/N$  vs  $\tau$  and (d)  $\langle V_x \rangle$  vs  $\tau$  for  $\phi = 0.12, 0.24, 0.36, 0.42, 0.48, 0.55, 0.61, 0.67, 0.73, 0.79$ , and  $0.85$  at  $A_p = 2.5$ , where there can be a transition from a reverse ratchet to a normal ratchet with increasing  $\tau$ . (b,e)  $C_L/N$  and  $\langle V_x \rangle$  vs  $A_p$  at  $\phi = 0.36$  for  $\tau = 100, 200, 400, 500, 600, 1000, 2500, 5000, 7500, 1 \times 10^4, 2 \times 10^4, 3 \times 10^4, 5 \times 10^4$ , and  $1 \times 10^5$ , showing that only a normal ratchet effect occurs. (c,f)  $C_L/N$  and  $\langle V_x \rangle$  vs  $A_p$  at  $\phi = 0.61$  for the same  $\tau$  values as in panels (b) and (e). Inset of (f): blow up of main panel showing a detail of the weak reverse ratchet effect that appears at large  $A_p$ .

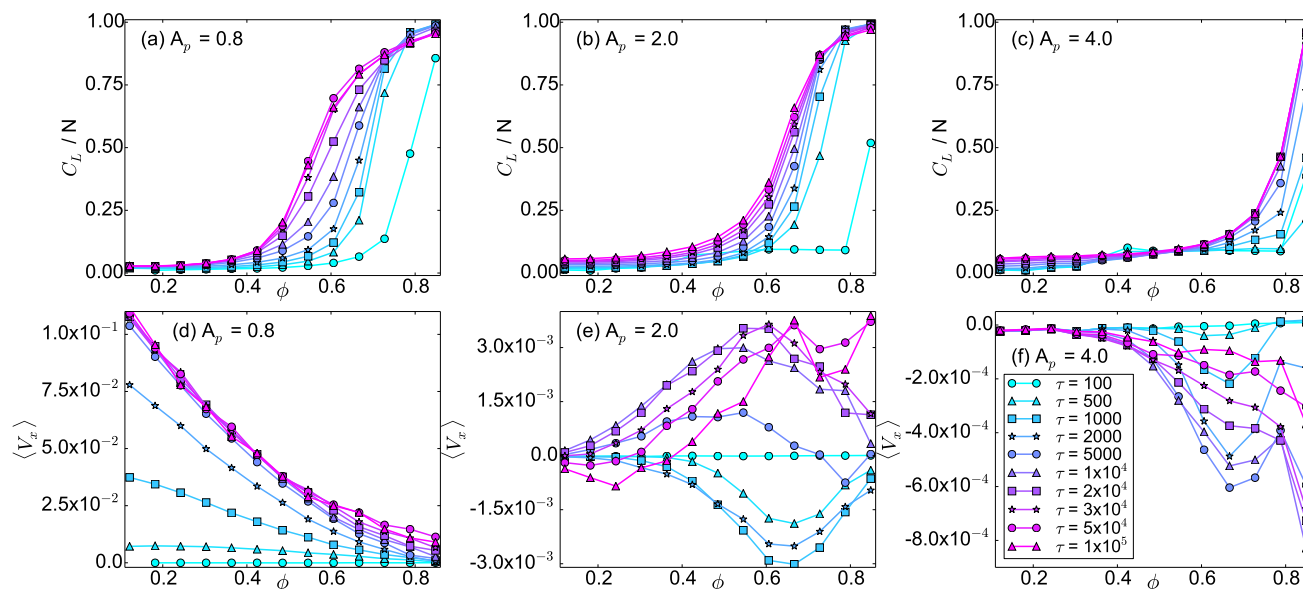


**Fig. 8** (a,b,c)  $C_L/N$  vs  $\tau$  and (d,e,f)  $\langle V_x \rangle$  vs  $\phi$  for  $\tau = 100, 500, 1000, 2000, 5000, 1 \times 10^4, 2 \times 10^4, 3 \times 10^4, 5 \times 10^4$ , and  $1 \times 10^5$  in samples with a substrate lattice constant of  $a = 2.0$ , twice as large as the lattice constant considered previously. (a,d)  $A_p = 0.8$ . (b,e) At  $A_p = 2.0$  a reverse ratchet effect occurs. (c,f) At  $A_p = 4.0$ , the magnitude of the reverse ratchet effect initially increases with increasing  $\tau$  for  $\tau < 1 \times 10^4$  and then decreases as  $\tau$  further increases.

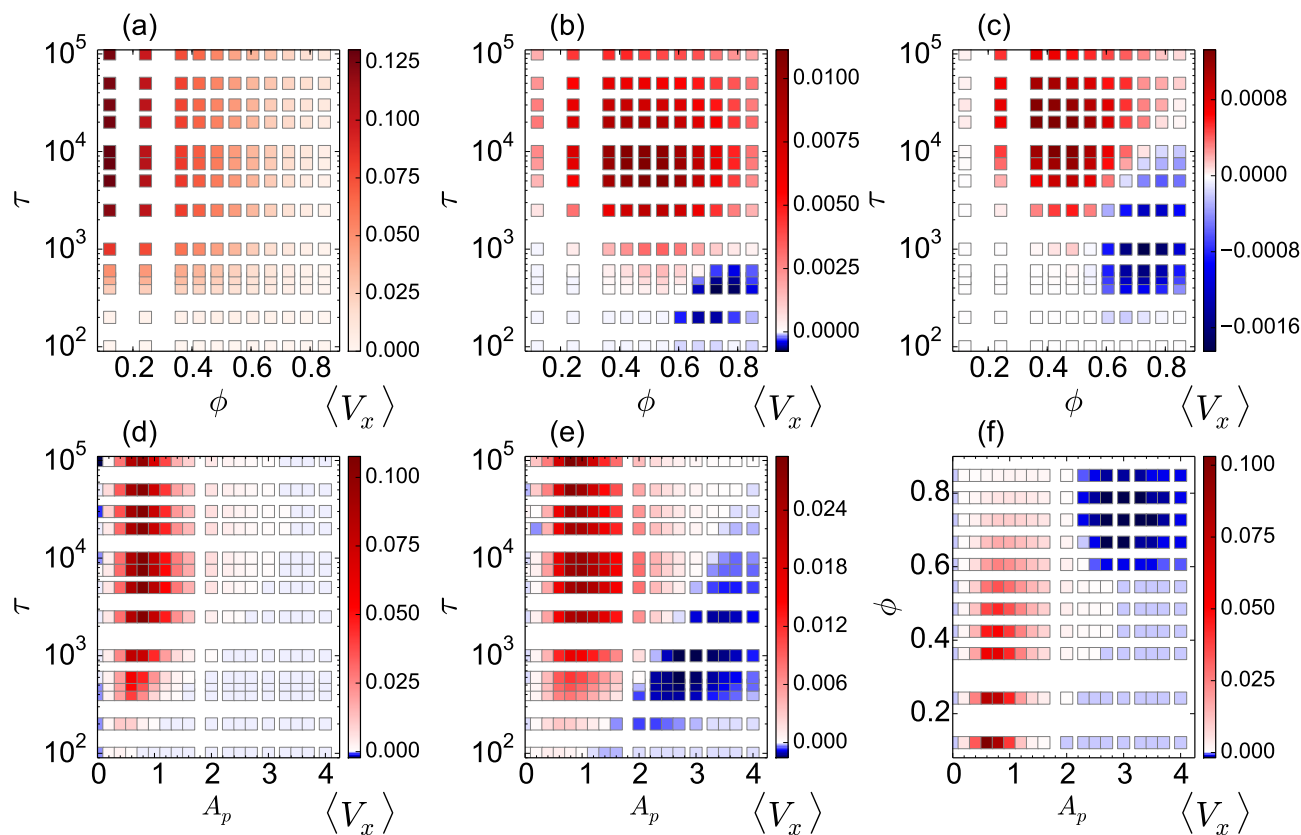


**Fig. 9** Phase diagrams in samples with  $a = 1.0$  showing the magnitude of the ratchet effect as determined by the value of  $\langle V_x \rangle$ , with blue denoting a reverse ratchet and red denoting a normal ratchet, as indicated by the color bar keys. (a,b,c)  $\tau$  vs  $\phi$  phase diagrams at (a)  $A_p = 0.8$ , (b)  $A_p = 2.0$ , and (c)  $A_p = 3.0$ . (d,e)  $\tau$  vs  $A_p$  phase diagrams at (d)  $\phi = 0.24$  and (e)  $\phi = 0.68$ . (f)  $\phi$  vs  $A_p$  phase diagram at  $\tau = 1000$ .



and as  $A_p$  increases,  $\langle V_x \rangle$  increases to a maximum value near  $A_p = 0.75$  before decreasing back to zero at higher  $A_p$ . The normal ratchet effect operates most efficiently when particles can overcome only the barrier for motion in the easy direction, and not the barrier in the hard direction. The particles can overcome the barrier in the easy direction when  $A_p \leq A_p^e$  with  $A_p^e = (3/2)F^m$ , and they can overcome the barrier in the hard direction when  $A_p \leq A_p^h$  with  $A_p^h = (3/4)F^m$ . Thus, the ratchet effect is zero for large  $A_p$ , becomes finite below  $A_p = A_p^e = 1.5$ , and diminishes rapidly below  $A_p \approx A_p^h = 0.75$ . In Fig. 7(c,f) at  $\phi = 0.61$ , increasing  $A_p$  decreases the cluster size  $C_L/N$  for  $\tau < 7.5 \times 10^4$  as the particles become increasingly localized, while at  $\tau = 1 \times 10^5$ ,  $C_L/N$  develops a small nonmonotonic peak near  $A_p = 1.5$ . For all  $\tau$ , there is still a local maximum in  $\langle V_x \rangle$  near  $A_p \approx 0.75$ , while for  $A_p > 2.0$  at low values of  $\tau$ , a weak reverse ratchet effect occurs.

We have also examined systems with different substrate periods  $a$ . We find that for larger values of  $a$ , the onset of the formation of multiple rows of particles in a single substrate minimum shifts to lower  $\phi$ , and that therefore the reverse ratchet regime is enhanced. In Fig. 8(a,d) we show  $C_L/N$  and  $\langle V_x \rangle$  versus  $\phi$  at  $A_p = 0.8$  for varied  $\tau$  in a sample with  $a = 2.0$ , twice as large as the lattice constant considered previously. For  $A_p < 1.0$ , there is a normal ratchet effect that generally decreases in magnitude with increasing  $\phi$  and that saturates in magnitude with increasing  $\tau$ . In Fig. 8(b,e), we plot the same quantities for  $A_p = 2.0$ , where the ratchet effect becomes non-monotonic and switches from a reverse ratchet for  $\tau < 5000$  to a normal ratchet for  $\tau \geq 5000$ . In contrast, for the  $a = 1.0$  system in Fig. 3 at the same value of  $A_p$ , there is almost no reverse ratchet regime. In Fig. 8(c,f), the  $C_L/N$  and  $\langle V_x \rangle$  versus  $\phi$  curves for  $a = 2.0$  at  $A_p = 4.0$  indicate that the ratchet effect is always in the reverse direction with a magnitude that increases with increasing  $\phi$ , a behavior that is the opposite of that observed at  $A_p = 0.8$ .

In Fig. 9 we highlight the different ratcheting behaviors for  $a = 1.0$  in a series of phase diagrams colored according to the value of  $\langle V_x \rangle$ , where blue indicates a reverse ratchet effect, white indicates no ratchet effect, and red indicates a normal ratchet effect. In Fig. 9(a) we show a  $\tau$  versus  $\phi$  phase diagram at  $A_p = 0.8$  where only a normal ratchet effect occurs. The ratchet efficiency decreases with decreasing  $\tau$  and increasing  $\phi$ . At  $A_p = 2.0$  in Fig. 9(b), the  $\tau$  versus  $\phi$  phase diagram plot indicates that the maximum normal ratchet effect appears near  $\phi = 0.5$  and  $\tau = 10^4$ , while reverse ratchet effects appear in the lower right hand corner at low  $\tau$  and large  $\phi$ . In Fig. 9(c), the  $\tau$  versus  $\phi$  phase diagram shows that the extent of the reversed ratchet regime is larger and that there is a clear transition from a reverse to a normal ratchet as a function of increasing  $\tau$  and/or decreasing  $\phi$ . As  $A_p$  is further increased, the reversed ratchet region grows, but the magnitude of the ratchet effect is generally reduced. In the  $\tau$  versus

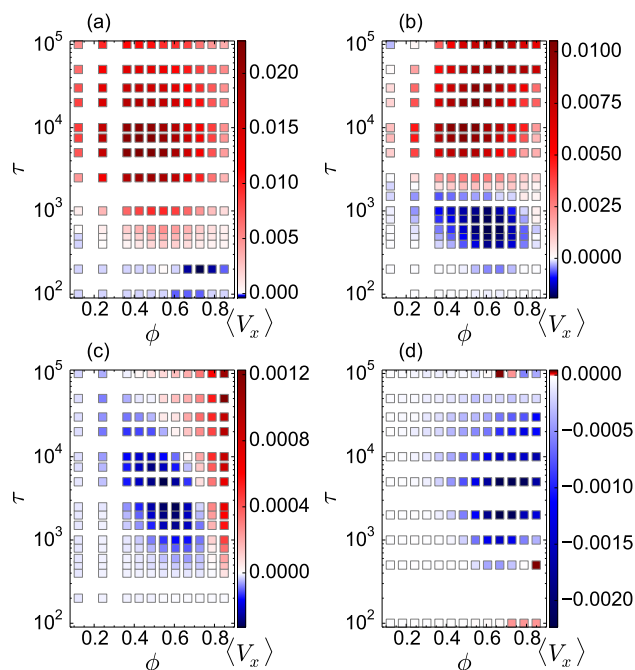


**Fig. 10** Phase diagrams as a function of  $\tau$  vs  $\phi$  showing the magnitude of the ratchet effect as determined by the value of  $\langle V_x \rangle$ , with blue denoting a reverse ratchet and red denoting a normal ratchet, as indicated by the color bar keys. (a) At  $A_p = 1.6$  and  $a = 1.0$ , there is a normal ratchet effect. (b) At  $A_p = 1.6$  and  $a = 2.0$ , there is a transition from a normal to a reverse ratchet effect. (c) At  $A_p = 3.0$  and  $a = 1.5$ , the reverse ratchet regime extends to higher values of  $\tau$ . (d) At  $A_p = 3.0$  and  $a = 2.0$ , the ratchet effect is predominately in the reverse direction.

$A_p$  phase diagram at  $\phi = 0.24$  in Fig. 9(d), the ratchet effect is always in the normal direction and is maximum in a band along the  $A_p = 0.8$  line. Regions of normal and reverse ratcheting appear in the  $\tau$  versus  $A_p$  phase diagram for  $\phi = 0.68$ , as shown in Fig. 9(e). In the  $\phi$  versus  $A_p$  phase diagram for fixed  $\tau = 1000$  in Fig. 9(f), a normal ratchet effect occurs for  $A_p < 2.0$ , while there is a transition to a reverse ratchet effect for  $A_p > 2.0$  and  $\phi > 0.5$ .

In Fig. 10(a) we show the ratchet phase diagram as a function of  $\tau$  versus  $\phi$  for a system with  $A_p = 1.6$  and  $a = 1.0$ , where the ratchet effect is always in the normal direction. For  $A_p = 1.6$  and  $a = 2.0$  in Fig. 10(b), at large  $\tau$  a normal ratchet effect occurs, as shown in Fig. 5(c) for  $\phi = 0.61$  and  $\tau = 1 \times 10^4$ , while at lower  $\tau$ , multiple rows of particles can be trapped in each substrate minimum, producing a region of reverse ratchet effect. At higher values of  $A_p$ , the size of the reverse ratchet effect region increases, as shown in Fig. 10(c) for  $A_p = 3.0$  and  $a = 1.5$ . In Fig. 10(d) at  $A_p = 3.0$  and  $a = 2.0$ , the ratchet effect is predominately in the reverse direction, as

illustrated in Fig. 5(d) for  $\phi = 0.72$  and  $\tau = 2500$ .

## 4 Summary

We show that in a 2D system of sterically interacting run-and-tumble disk-shaped particles in the presence of a quasi-one-dimensional asymmetric periodic substrate, a variety of collective active ratchet behaviors can occur, including nonmonotonic changes in the ratchet effect magnitude as well as ratchet reversals. A normal ratchet effect, where a net drift of the particles occurs along the easy flow direction of the substrate, appears for weak substrates, and the ratchet efficiency generally decreases with increasing particle density due to self-jamming or clustering effects since it is more difficult for a cluster to undergo ratcheting motion than for individual particles to do so. For intermediate substrate strengths, the ratchet efficiency is nonmonotonic as function of particle density or activity. At low particle densities, individual particles cannot jump over the potential barrier, but particle-particle interactions can produce a collective particle hopping in the easy direction of the substrate asymmetry. When the particle density or activity is high enough, strong clustering effects occur that reduce the ratchet efficiency. For strong substrates where multiple rows of particles can form in each substrate minimum, it is possible to realize a reverse ratchet effect in which the net flux of particles is in the hard direction of the substrate asymmetry. The size of the reverse ratchet regime can be increased by increasing the size of the substrate periodicity, which shifts the transition from single to multiple rows of particles per substrate minimum to lower particle densities. Our work shows that by exploiting collective effects, it is possible to create reversible active matter ratchets which could be useful for various sorting applications.

## 5 Acknowledgements

This work was carried out under the auspices of the NNSA of the U.S. DoE at LANL under Contract No. DE-AC52-06NA25396. The work of DM was supported in part by the U.S. DoE, Office of Science, Office of Workforce Development for Teachers and Scientists (WDTs) under the Visiting Faculty Program (VFP).

## References

- 1 P. Reimann, *Phys. Rep.*, 2002, **361**, 57.
- 2 H. Linke, *Appl. Phys. A*, 2002, **75**, 167.
- 3 P. Hänggi and F. Marchesoni, *Rev. Mod. Phys.*, 2009, **81**, 387.
- 4 J. Rousselet, L. Salome, A. Ajdari, and J. Prost, *Nature (London)*, 1994, **370**, 446.
- 5 C.S. Lee, B. Jankó, I. Derényi, and A.L. Barabási, *Nature (London)*, 1999, **400**, 337.
- 6 J. F. Wambaugh, C. Reichhardt, C.J. Olson, F. Marchesoni, and F. Nori, *Phys. Rev. Lett.*, 1999, **83**, 5106.
- 7 A. Pérez-Junquera, V.I. Marconi, A.B. Kolton, L.M. Álvarez-Prado, Y. Souche, A. Alija, M. Vélez, J.V. Anguita, J.M. Alameda, J.I. Martín, and J.M.R. Parrondo, *Phys. Rev. Lett.*, 2008, **100**, 037203.
- 8 J.H. Franken, H.J.M. Swagten, and B. Koopmans, *Nature Nanotechnol.*, 2012, **7**, 499.
- 9 M.T. Downton, M.J. Zuckermann, E.M. Craig, M. Plischke, and H. Linke, *Phys. Rev. E*, 2006, **73**, 011909.
- 10 M. Kenward and G. Slater, *Phys. Rev. E*, 2008, **78**, 051806.
- 11 Z. Farkas, P. Tegzes, A. Vukics, and T. Vicsek, *Phys. Rev. E*, 1999, **60**, 7022.
- 12 J.F. Wambaugh, C. Reichhardt, and C.J. Olson, *Phys. Rev. E*, 2002, **65**, 031308.
- 13 P.H. Jones, M. Goonasekera, and F. Renzoni, *Phys. Rev. Lett.*, 2004, **93**, 073904.
- 14 C. Reichhardt and C.J. Olson Reichhardt, *Phys. Rev. E*, 2003, **68**, 046102.
- 15 D. Speer, R. Eichhorn, and P. Reimann, *Phys. Rev. Lett.*, 2009, **102**, 124101.
- 16 P. Tierno and T.M. Fischer, *Phys. Rev. Lett.*, 2014, **112**, 048302.
- 17 I. Derényi and T. Vicsek, *Phys. Rev. Lett.*, 1995, **75**, 374.
- 18 J.E. Villegas, S. Savelev, F. Nori, E.M. Gonzalez, J.V. Anguita, R. Garcia, and J.L. Vicent, *Science*, 2003, **302**, 1188.
- 19 C.C. de Souza Silva, J. Van de Vondel, M. Morelle, and V.V. Moshchalkov, *Nature (London)*, 2006, **440**, 651.
- 20 V.I. Marconi, *Phys. Rev. Lett.*, 2007, **98**, 047006.
- 21 Q. Lu, C.J. Olson Reichhardt, and C. Reichhardt, *Phys. Rev. B*, 2007, **75**, 054502.
- 22 D. Perez de Lara, M. Erekhinsky, E.M. Gonzalez, Y.J. Rosen, I.K. Schuller, and J.L. Vicent, *Phys. Rev. B*, 2011, **83**, 174507.
- 23 M.C. Marchetti, J.F. Joanny, S. Ramaswamy, T.B. Liverpool, J. Prost, M. Rao, and R.A. Simha, *Rev. Mod. Phys.*, 2013, **85**, 1143.
- 24 M.E. Cates, *Rep. Prog. Phys.*, 2012, **75**, 042601.
- 25 C. Bechinger, R. Di Leonardo, H. Löwen, C. Reichhardt, G. Volpe, and G. Volpe, arXiv:1602.00081 (unpublished).
- 26 P. Galajda, J. Keymer, P. Chaikin, and R. Austin, *J. Bacteriol.*, 2007, **189**, 8704.
- 27 M.B. Wan, C.J. Olson Reichhardt, Z. Nussinov, and C. Reichhardt, *Phys. Rev. Lett.*, 2008, **101**, 018102.
- 28 J. Tailleur and M.E. Cates, *Europhys. Lett.*, 2009, **86**, 60002.
- 29 L. Angelani, A. Costanzo, and R. Di Leonardo, *Europhys. Lett.*, 2011, **96**, 68002.
- 30 C.J. Olson Reichhardt and C. Reichhardt, arXiv:1604.01072 (unpublished).
- 31 V. Kantsler, J. Dunkel, M. Polin, and R. E. Goldstein, *Proc. Natl. Acad. Sci. (USA)*, 2013, **110**, 1187.
- 32 A. Pototsky, A. M. Hahn, and H. Stark, *Phys. Rev. E*, 2013, **87**, 042124.
- 33 B. Ai, Q. Chen, Y. He, F. Li, and W. Zhong, *Phys. Rev. E*, 2013, **88**, 062129.
- 34 E. Yariv and O. Schnitzer, *Phys. Rev. E*, 2014, **90**, 032115.
- 35 I. Berdakin, Y. Jeyaram, V.V. Moshchalkov, L. Venken, S. Dierckx, S.J. Vanderleyden, A.V. Silhanek, C.A. Condat, and V.I. Marconi, *Phys. Rev. E*, 2013, **87**, 052702.
- 36 C. Reichhardt and C. J. Olson Reichhardt, *Phys. Rev. E*, 2013, **88**, 062310.
- 37 F.Q. Potiguar, G.A. Farias, and W.P. Ferreira, *Phys. Rev. E*, 2014, **90**, 012307.
- 38 B.-Q. Ai and J.-C. Wu, *J. Chem. Phys.*, 2014, **140**, 094103.
- 39 M.-B. Wan and Y. Jho, *Soft Matter*, 2013, **9**, 3255.
- 40 P.K. Ghosh, V.R. Misko, F. Marchesoni, and F. Nori, *Phys. Rev. Lett.*, 2013, **110**, 268301.
- 41 N. Koumakis, A. Lepore, C. Maggi, and R. Di Leonardo, *Nature Commun.*, 2013, **4**, 2588.

- 
- 42 R. Di Leonardo, L. Angelani, D. Dell'Arciprete, G. Ruocco, V. Iebba, S. Schippa, M.P. Conte, F. Mecarini, F. De Angelis, and E. Di Fabrizio, *Proc. Natl. Acad. Sci. (USA)*, 2010, **107**, 9541.
- 43 A. Sokolov, M.M. Apodaca, B.A. Grzybowski, and I.S. Aranson, *Proc. Natl. Acad. Sci. (USA)*, 2010, **107**, 969.
- 44 A. Kaiser, K. Popowa, H.H. Wensink, and H. Löwen, *Phys. Rev. E*, 2013, **88**, 022311.
- 45 A. Kaiser, A. Peshkov, A. Sokolov, B. ten Hagen, H. Löwen, and I.S. Aranson, *Phys. Rev. Lett.*, 2014, **112**, 158101.
- 46 S.A. Mallory, C. Valeriani, and A. Cacciuto, *Phys. Rev. E*, 2014, **90**, 032309.
- 47 J. Tailleur and M.E. Cates, *Phys. Rev. Lett.*, 2008, **100**, 218103.
- 48 Y. Fily and M.C. Marchetti, *Phys. Rev. Lett.*, 2012, **108**, 235702.
- 49 G.S. Redner, M.F. Hagan, and A. Baskaran, *Phys. Rev. Lett.*, 2013, **110**, 055701.
- 50 J. Palacci, S. Sacanna, A.P. Steinberg, D.J. Pine, and P.M. Chaikin, *Science*, 2013, **339**, 936.
- 51 I. Buttinoni, J. Bialké, F. Kümmel, H. Löwen, C. Bechinger, and T. Speck, *Phys. Rev. Lett.*, 2013, **110**, 238301.
- 52 C. Reichhardt and C. J. Olson Reichhardt, *Phys. Rev. E*, 2014, **90**, 012701.
- 53 T. Vicsek, A. Czirók, E. Ben-Jacob, I. Cohen, and O. Shochet, *Phys. Rev. Lett.*, 1995, **75**, 1226.
- 54 J.A. Drocco, C.J. Olson Reichhardt, and C. Reichhardt, *Phys. Rev. E*, 2012, **85**, 056102.
- 55 G. Mahmud, C.J. Campbell, K.J.M. Bishop, Y.A. Komarova, O. Chaga, S. Soh, S. Huda, K. Kandere-Grzybowska, and B.A. Grzybowski, *Nature Phys.*, 2009, **5**, 606.
- 56 S. Luding and H.J. Herrmann, *Chaos*, 1999, **9**, 673.